



High visible light-driven photocatalytic activity of large surface area Cu doped SnO₂ nanorods synthesized by novel one-step microwave irradiation method

M. Parthibavarman¹ · S. Sathishkumar² · S. Prabhakaran³ · M. Jayashree¹ · R. BoopathiRaja¹

Received: 20 May 2018 / Accepted: 7 August 2018 / Published online: 11 August 2018
© Iranian Chemical Society 2018

Abstract

The paper investigates the structural, optical and photocatalytic activity of large surface area single crystalline copper (Cu) doped SnO₂ nanorods (NRs) synthesized by a novel one-step microwave irradiation method. Powder X-ray diffraction (XRD) analysis confirms that both pure and Cu doped SnO₂ are tetragonal rutile type structure (space group P42/mmm) formed during the microwave process within 10 min without any post annealing treatment. Transmission electron microscopy (TEM) reveals that the as synthesized Cu doped SnO₂ samples exhibited rod-like shape and the length was less than 80 nm and diameter was about few nanometers. Typical selected-area electron diffraction (SAED) pattern indicates that, the growth direction of Cu–SnO₂ nanorod is along [110] direction. The variety of phonon interaction in the pure and Cu doped SnO₂ is observed by Raman spectroscopy. Electron paramagnetic resonance and X-ray photoelectron spectroscopy (XPS) confirms that the presence of copper and tin as Cu²⁺ and Sn⁴⁺ in state, respectively. The photocatalytic activity was monitored via the degradation of methylene blue (MB) and Rhodamine B (RhB) dyes and the Cu–SnO₂ showed better photocatalytic activity than that of pure SnO₂. This could be attributed to the effective electron–hole separation by surface modification.

Keywords Metal oxide semiconductors · SnO₂ · Cu doping · Nanorods · Microwave · Photocatalyst

Introduction

Recently, oxide-based semiconducting photocatalyst has been paid great attention for the degradation and purification of variety of organic pollutants (dyes, phenols, pesticides and pharmaceuticals) in aqueous media [1]. Among different types of metal oxide semiconductors, TiO₂ [2], ZnO [3], WO₃ [4], Fe₂O₃ [5] and Bi₂O₃ [6] are extensively studied photocatalysts suitable to their band gap, non-toxicity, chemical stability, and inertness. Tin oxide (SnO₂) is the most consistent and essential wide band gap semiconductor after TiO₂. It has superior physic-chemical properties,

enhanced visible light absorptions, extreme catalytic activity under UV–visible light to degrade pollutants, outstanding resistivity variation in different gas, good sensitivity and stability [7]. Because of eco-friendly and high-photocatalytic behavior of SnO₂, it has mainly used for ideal photocatalyst for solar energy conversion. But still, the photocatalytic efficiency of pure SnO₂ is inadequate by many factors, like its wide band gap (3.6 eV), rapid recombination rate of electron–hole pairs, and low surface area. Due to its wide band gap, it is not expert to consume the full range of the solar spectrum. To conquer this problem much effort has been devoted to modifying the surface or bulk properties of SnO₂, such as doping with metal ions (V [8], Ag [9], Cu [10]) or non-metal ions (N, S, C) [11] or by combining SnO₂ with another semiconductor. Generally, copper (Cu) is most suitable dopant to improve the photocatalytic properties of SnO₂ under visible light. Even though, only few reports are existing for photocatalytic performance Cu doped SnO₂. Most of the literatures focus on gas sensing performance of Cu or CuO doped SnO₂. An attempt to further growth in the photocatalytic performance, here we have choosing Cu dopant. It is well known that the doping of Cu ions in the

✉ M. Parthibavarman
varmanphysics85@gmail.com

¹ PG and Research Department of Physics, Chikkaiah Naicker College, Erode, Tamilnadu 638 004, India

² Research and Development Centre, Bharathiar University, Coimbatore, Tamilnadu 641 046, India

³ Centre for Crystal Growth, VIT University, Vellore, Tamilnadu 632 014, India

SnO₂ nanostructure is a very useful way to inhibit the charge recombination and tuning band gap of pristine SnO₂.

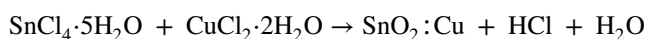
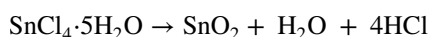
Many synthesis methods have been adapted for to prepare the nanostructure Cu doped SnO₂, such as: chemical precipitation, sol–gel, hydrothermal, solvothermal, thermal evaporation and micro emulsion methods etc. Among these, microwave energy-alone or in combination with conventional energy sources makes it possible to control the drying process more precisely to obtain greater yields and better quality products in the shortest possible time [12]. In the present investigation consists of microwave assisted pure and Cu doped SnO₂ single crystalline nanorods and their structural, optical and photocatalytic activity. To the best of the author's knowledge this is the first preliminary report about photocatalytic performance of large method.

Experimental procedure

Preparation of Cu doped SnO₂ nanorods

All the chemicals used were of analytical grade and were used as received without any further purification. In a typical synthesis, 2.25 g of SnCl₄·5H₂O was dissolved in 50 mL deionized water under magnetic stirring for 30 min. CuCl₂·2H₂O were mixed at a stoichiometric ratio with different concentrations (0.01, 0.05, and 0.10 mol%) of copper chloride dihydrate (CuCl₂·2H₂O) and dissolved in DI water and stirred for another 30 min. The NH₄OH (as precipitate agent) solution was added drop wise until the pH value reaches to 10. After complete this process a white color suspension was obtained. This solution was centrifuged and washed with ethanol and DI water more than five times to remove the Cl⁻ and NH₄⁺ ions. The sol was transferred into Teflon lined household microwave oven (2.45 GHz) with power 900 W (120 °C) and irradiated for 15 min. The preparation of pure SnO₂ was followed by a same procedure except Cu source. The final product was grey and light green for pure and Cu doped SnO₂, respectively. The samples with pure and 0.01, 0.05, and 0.10 mol % Cu named as Sn, Cu 1, Cu 5 and Cu 10, respectively.

The possible chemical reaction that takes place on the heated surface to produce SnO₂ and Cu doped SnO₂ (SnO₂:Cu) may be as follows:



Characterization details

Powder X-ray diffraction method with Rigaku X-ray diffractometer with monochromatic CuK α radiation of wavelength 1.5406 Å was used to analyze the crystallographic

nature and grain size of the as synthesized products. The microstructure and elemental composition of the samples were analyzed by using scanning electron microscope (JEOL Model JSM—6390LV) and energy dispersive spectra (EDS) (JEOL Model JED—2300) analysis. Transmission electron microscopy (TEM), selected-area electron diffraction (SAED), and high-resolution transmission electron microscopy (HRTEM) measurements were performed on an FEI Tecnai F20 microscope at 200 kV. The fundamental vibration modes of the samples were measured by using Raman spectra of the samples were recorded using BRUKER RFS 27: Stand alone FT-Raman Spectrometer at a resolution of 0.2 cm⁻¹. UV–VIS diffusion reflectance spectroscopy equipped with CARY 5E UV–VIS–NIR spectrophotometer (wavelength range of 200–900 nm) was used to analyze the band gap and optical nature of the samples. Photoluminescence spectra of the samples were measured using PerkinElmer LS 55 spectrometer equipped with a He–Cd laser source (325 nm as excitation wavelength). XPS was analyzed by using a Thermo Scientific K-alpha surface analysis instrument.

Photocatalytic activity set up

The detailed photocatalytic set up was described in our previous published work [13]. We also investigated the photocatalytic property of methylene blue (MB) using Cr doped WO₃ catalyst powders synthesized by microwave irradiation technique [14]. In this photocatalytic set up, 500 W halogen lamp was used as the visible light source to trigger the photocatalytic reaction. The photocatalytic reactor consists of a specially designed quartz glass cylinder (30 cm width and 40 cm height). In the process of photocatalytic, the relevant dye solutions like MB and RhB (10 mg L⁻¹, 25 μM) was stirred with the 0.1 g of catalyst powder sample (Cu–SnO₂) in the dark for 30 min to achieve adsorption equilibrium, prior to irradiation under visible light. The visible light irradiation time was varied from different timings (20, 40, 60, ..., 120 min) with a regular interval of 20 min. The UV–Vis–NIR measurement was performed using PerkinElmer lambda 25 spectrophotometer to determine the absorption. The halogen lamp was placed at 15 cm away from the reactor during the irradiation. The degradation of MB and RhB was calculated using the ratio of initial (C₀) and final (C) concentration.

Results and discussion

XRD analysis

XRD is one of the essential tools to examine the structural perfection and product purity of the crystalline materials.

Figure 1a shows the powder XRD pattern of pure and Cu doped SnO_2 nanoparticles with different Cu concentrations. All the sharp diffraction peaks in both pure and Cu doped SnO_2 samples can be identified as tetragonal rutile phase of SnO_2 with lattice parameters match to reported values (JCPDS file no. 41-1445). No other impurity-related characteristics peaks (Cu or CuO) are detected, this proves that phase purity of the samples. When the Cu dopant concentration increases, the diffraction peaks shift towards the higher angles side (Fig. 1b), but the peaks intensity was broaden and suppressed, this may probably due to decreasing the grain size and crystallinity. Figure 1c shows the variation of peak intensity along (110) plane with different Cu concentrations from 0.1 mol% to 1 mol%. With the increase of Cu content, the peak position of (110) plane shifts towards the higher angles compared with the undoped SnO_2 . Moreover,

the calculated lattice parameters and volume of the pure SnO_2 was decreases with the increase of Cu concentrations (Table 1). This might be due to the smaller ionic radius of Cu^{2+} (0.57 Å) than Sn^{4+} (0.69 Å) [15]. The smaller crystallite size offer high-surface area and oxygen vacancies,

Table 1 Shows the average grain size, lattice parameters and volume of pure and Cu doped SnO_2

| Sample | Crystallite size (nm) | Lattice parameters | | Cell volume (Å ³) |
|--------|-----------------------|--------------------|--------|-------------------------------|
| | | a (Å) | b (Å) | |
| Sn | 27 | 4.7466 | 3.1907 | 71.88 |
| Cu 1 | 23 | 4.7327 | 3.1901 | 71.45 |
| Cu 5 | 20 | 4.7298 | 3.1879 | 71.31 |
| Cu 10 | 14 | 4.7201 | 3.1801 | 70.84 |

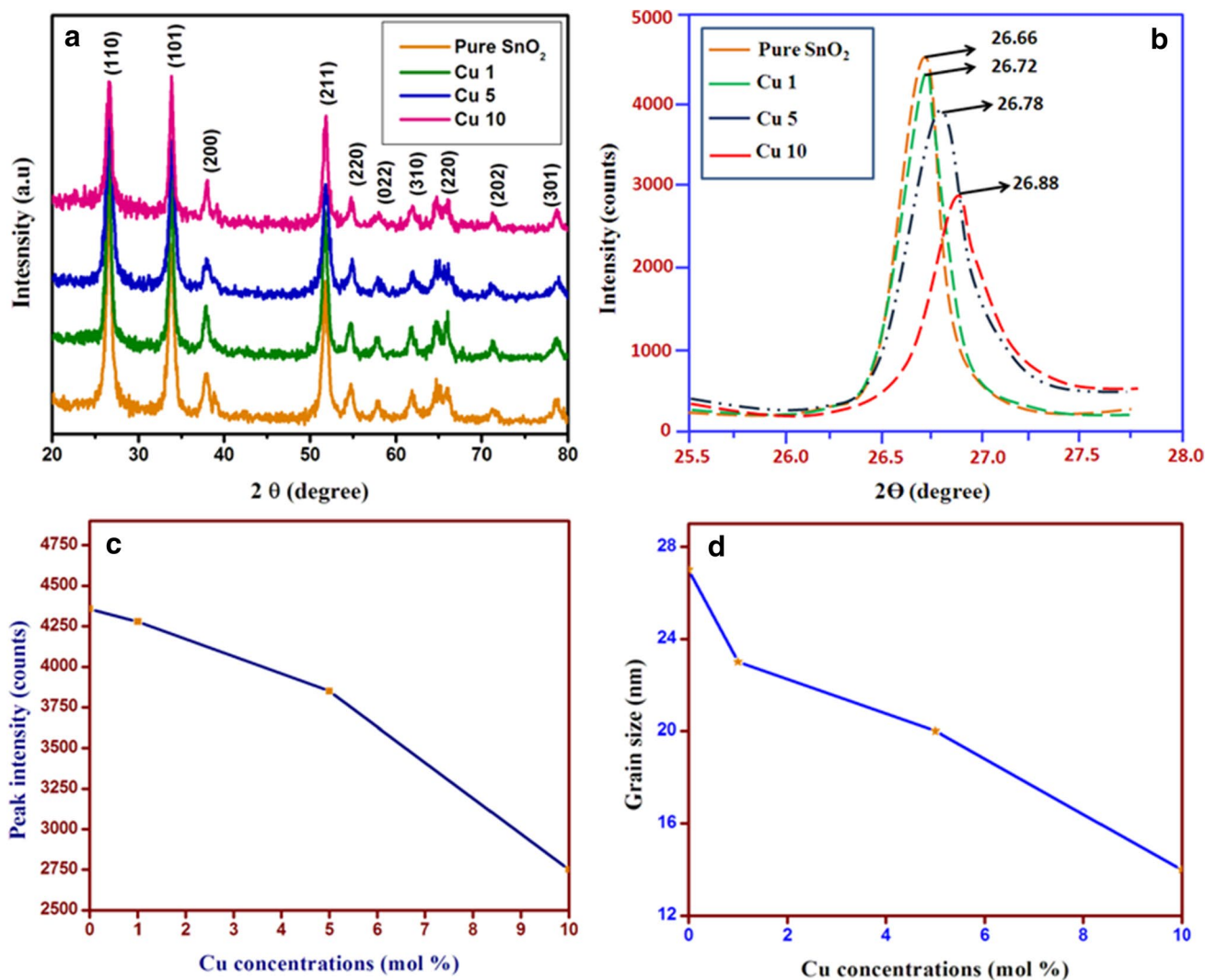


Fig. 1 a Powder XRD pattern of pure and Cu doped SnO_2 nanoparticles. b Magnified and high-resolution XRD pattern of the nanoparticles between 25.6° and 27° along (110) plane. c Variation of peak

intensity along (110) plane as a function of Cu concentrations. d Change in average grain size as a function of Cu concentrations

which results in improve the photocatalytic performance. Figure 1d shows the decrease in grain size as a function of Cu concentrations. The average grain size was calculated from Debye scherrer's formula [16] and found to decreased from 27 to 14 nm with the increase of Cu concentrations (0.01–0.10 mol%). The decrease in crystalline size due to grain growth of pure SnO₂ is suppressed by Cu dopant and confirms the substitution of Cu²⁺ in regular lattice site of SnO₂.

SEM analysis

The surface morphology plays an important role in the photocatalytic activity of semiconductor nanoparticles. The morphology of the pure and Cu doped SnO₂ nanoparticles was determined by SEM micrographs as depict in Fig. 2. The morphology of the pure SnO₂ was found to nearly spherical shaped particles and their aggregates (Fig. 2a). It can be clearly seen that Cu doping leads to significant changes in the morphology of the synthesized SnO₂ nanostructures. The morphology changes from spherical to nanorods upon Cu doping can be clearly seen from Fig. 2b–d. This could be attributed to orientation attachments of Cu with SnO₂ nanoparticles.

EDS analysis

To verify the compositional elements present in the samples, EDS analysis was carried out for pure and Cu doped SnO₂ samples and the spectra were presented as shown in Fig. 2e–h. The sample mostly composed of Cu, Sn, O elements for different Cu concentrations from 0 to 10%. The presence of Cu element confirms that Cu doping into SnO₂ structure. It was also noticed that the percentage of Cu element peak is increased by Cu concentrations (Inset Fig. 2). Therefore, the calculated atomic percentage is nearly equal to their nominal stoichiometry within the experimental error.

TEM analysis

Figure 3 shows the TEM images of pure and Cu doped SnO₂ samples. It also confirms that the nanorods are formed with Cu doping. It can be seen that pure SnO₂ was spherical shaped morphology with average diameter of around 25–30 nm (Fig. 3a). The corresponding ring like patterns indicates existence of crystallites in all possible orientations (Fig. 3b). The halo rings are indexed as (110), (101), (200) and (211) planes which correspond to the rutile SnO₂ phase. Figure 3c shows the high-resolution TEM image of Cu doped SnO₂ single nanorod. The typical length of as synthesized single nanorod is around 75–85 nm and the width is around 20–30 nm. The lattice fringes in the HRTEM image (Fig. 3d) give clear evidence about the single crystal nature

of the Cu–SnO₂ nanorod. The spacing between adjacent lattice planes is 0.338 nm corresponding to (110). In addition, the presence of bright spots in the selected-area electron diffraction (SAED) pattern from an individual nanorod confirms that the rutile type SnO₂ with single crystalline in nature and the preferential growth along the [110] direction (inset of Fig. 3d).

Raman spectra analysis

Raman spectroscopy is preferably appropriate for the analysis of crystallographic knowledge and confinement of phonons in the samples. Figure 4a shows the Raman spectra of pure and Cu doped SnO₂ nanoparticles. The spectra of pure SnO₂ exhibited three peaks at 471, 642 and 782 cm⁻¹, which corresponding to the fundamental modes E_g, A_{2g} and B_{2g} characteristic of tetragonal phase of SnO₂ [17, 18]. It was clearly seen that the peak was shifted and broadening the intensity with the increase of Cu content. This could be attributed to decrease in grain size of pure SnO₂ and also morphology transformation of nanorods in the Cu doped SnO₂ samples. The decrease in grain size with increase in Cu doping is also confirmed by our XRD results. In addition that this phenomenon is owing to phonon scattering is take place in center of Brillouin zone which results in the form of symmetry-forbidden modes. So our Raman spectra again confirm the substitution of Cu²⁺ in the SnO₂ crystal structure.

UV-DRS spectra analysis

Figure 4b shows the UV-DRS spectra of pure and Cu doped SnO₂ nanoparticles. For pure SnO₂ sample, the absorption edge was found to be 365 nm, the edge was further shift towards longer wavelength upon doping by Cu. A considerable red shift and decreasing the band gap of pure SnO₂ was already observed by other TM-doped SnO₂ nanostructures [19, 20]. To further confirm the relation between doping and band gap (E_g), we have using Kubelka–Munk (K–M) model [14] is described below. The K–M model at any wavelength is given by $F(R_{\infty}) = (1 - R)^2/2R$, where R is the percentage of reflectance. A graph is plotted between $[F(R_{\infty})/hv]^2$ vs. hv and the intercept value is the direct band gap energy (Fig. 4c) [21]. The band gap energy was found to be 3.66, 3.54, 3.41 and 3.28 eV for Sn, Cu 1, Cu 5 and Cu 10 samples, respectively.

Photoluminescence spectra analysis

It is well known that PL spectroscopy is useful technique to investigate crystalline quality, surface defects, energy bands and excitation fine structure of the nanomaterials [22]. Figure 5a shows the room temperature PL emission

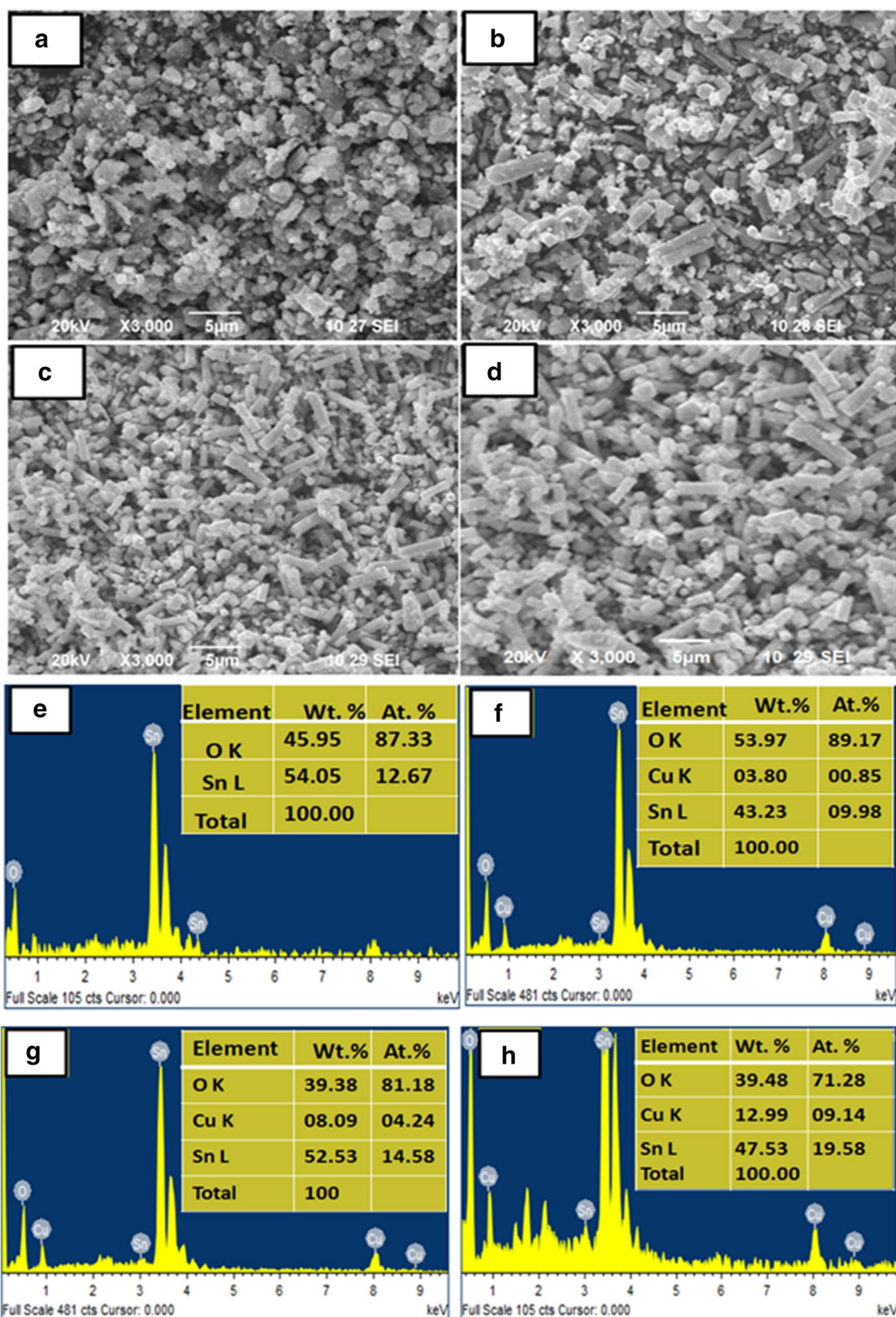
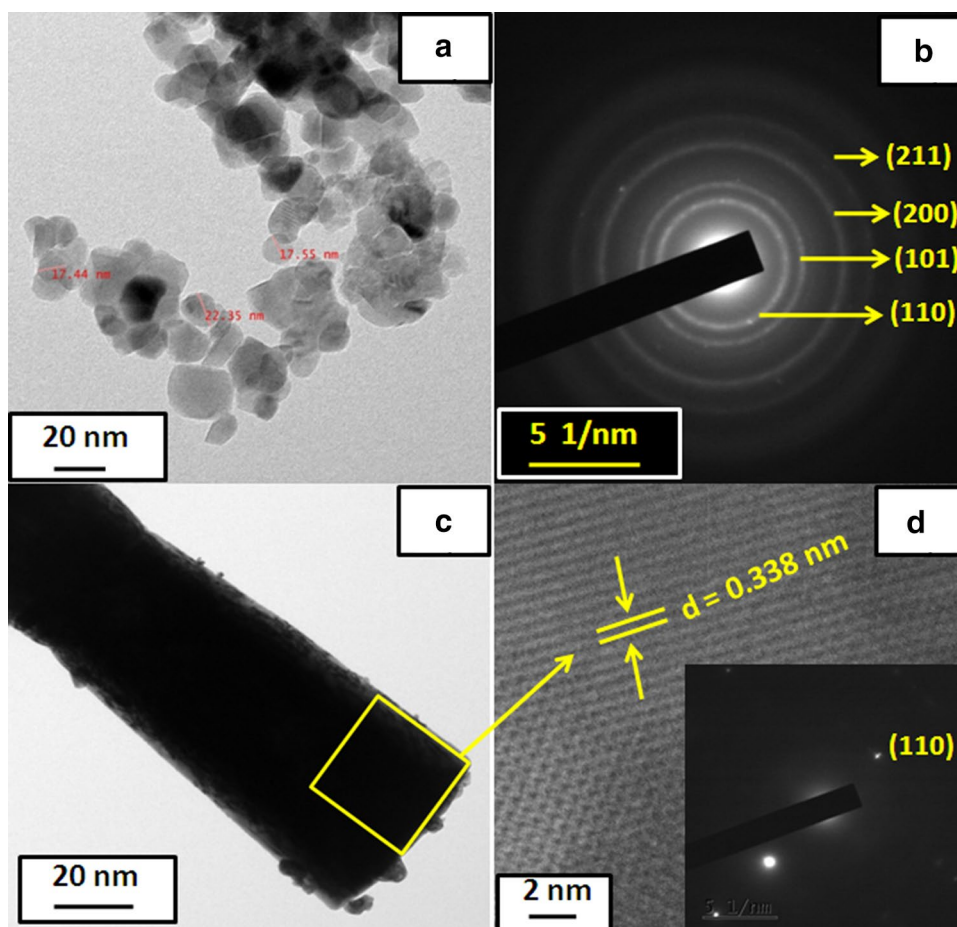


Fig. 2 SEM images of a pure SnO_2 , b Cu 1, c Cu 5, d Cu 10; EDS spectra of e pure SnO_2 , f Cu 1, g Cu 5, h Cu 10

Fig. 3 TEM image of **a** pure SnO₂, **b** corresponding SAED pattern, **c** TEM image of Cu 10 sample, **d** corresponding HRTEM and SAED pattern along [110] direction



spectra of the Cu doped SnO₂ nanoparticles. It can be seen that there are serious of emission peaks were observed at 362 nm, 376 nm (UV emission), 437 nm (blue emission) and 491 nm (green emission) of pure SnO₂ nanoparticles. The UV emission can be attributed to the near band edge emission (NBE) coming from the holes in the valence band and radiative recombination of electrons in the conduction band [23]. The blue and green emission peaks are might be due to the electron transition mediated by defect levels in the band gap and oxygen vacancies (V_{O}^{++} luminescent centers from V_{O}^{+}) [24]. It was noticed that a slight red shifting of peaks and enhance the intensity were observed for Cu doping, this could be attributed the case to defective energy levels introduced by Cu doping.

Electron paramagnetic resonance spectra (EPR) analysis

EPR spectra of Cu doped SnO₂ have been recorded at room temperature, using Varian E 112, operating at X-band frequency 8.5–9.5 GHz. Figure 5 b shows the broad EPR signal for pure Cu doped SnO₂ samples (Cu 1, Cu 5, and Cu 10). Generally EPR powder spectrum of copper gives four lines

corresponding to the parallel hyperfine splitting of the copper nucleus ($I = 3/2$) but it gives single broad EPR signal is due to exchange interaction. The parameter ‘g’ with is determined according to the equation $g = h\nu/\mu_B H_r$, where h is Planck’s constant, ν is the microwave frequency and μ_B is the Bohr magnetron. The g value calculated from this powder spectrum was 2.06, which indicate an axial symmetry with elongated tetragonal–octahedral due to broadening of line width which is due to exchange interactions. This similar finding was observed in Cu²⁺ doped ZnO [25]. The above information confirms that the Cu²⁺ ion doped substitutionally in tetragonal rutile structure of SnO₂.

XPS analysis

The XPS was carried out to confirm the valance state of Cu ions in the Cu doped SnO₂ and depict in Fig. 6a along with the core level spectra of Sn 3d, Cu 2p, and O1s peaks are shown in Fig. 6b–d, respectively. It was seen that a doublet at 480.4 and 490.3 eV can be assigned to Sn3d_{5/2} and Sn3d_{3/2}, respectively, as shown in Fig. 6a, which indicates that the Sn atoms are in 4⁺ state. The XPS spectrum of Cu 2p showed that a strong peak appeared at 938.1 eV, which

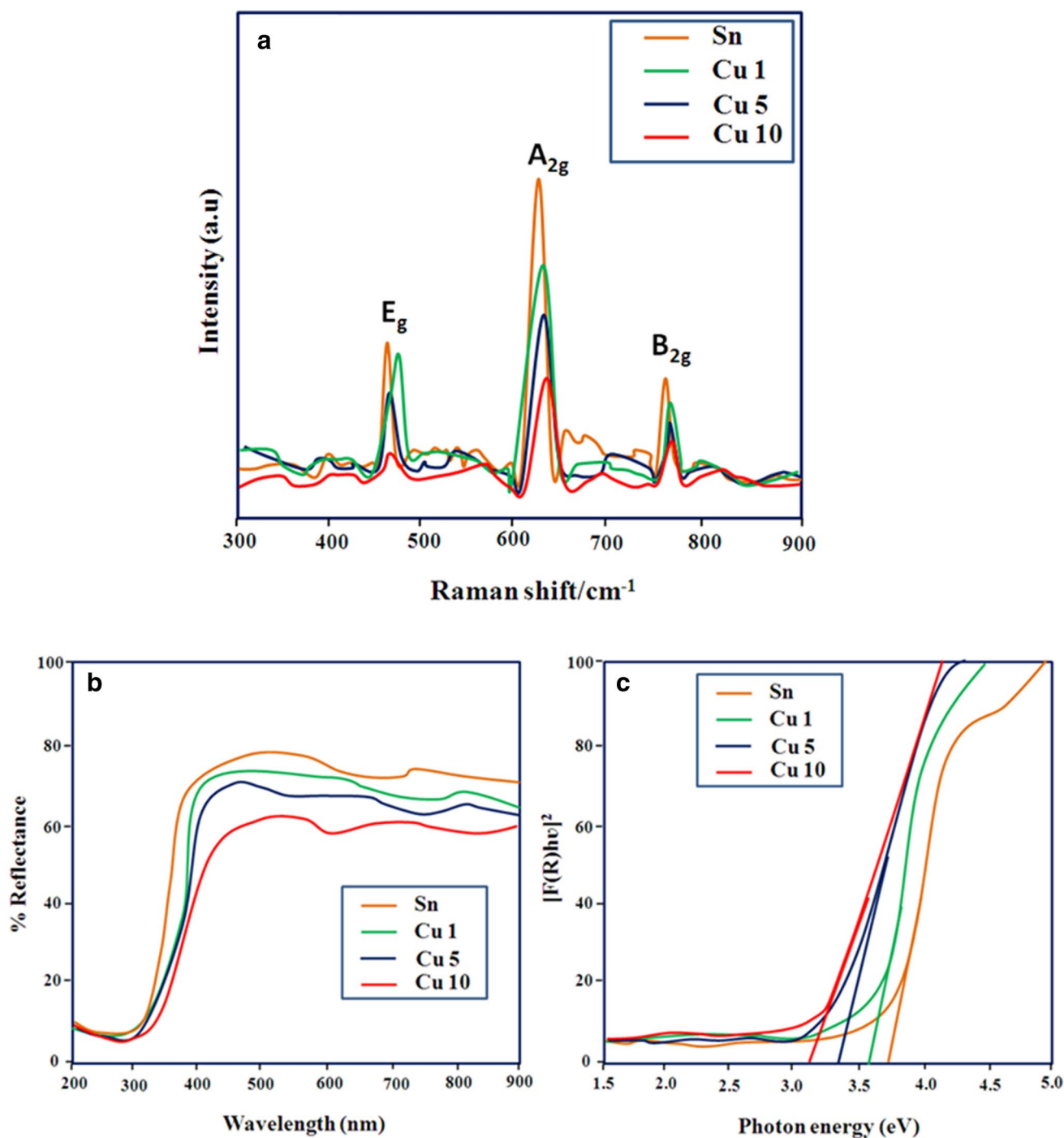


Fig. 4 **a** Raman spectra of pure and Cu doped SnO₂ nanoparticles; UV-DRS spectra of pure and Cu doped SnO₂ nanoparticles. **b** Reflectance spectra. **c** K–M Model

can be owing to the Cu 2p_{3/2} (Cu²⁺ state). The O1s peaks are located at 532.3 eV, which corresponds to O²⁻ ions in SnO₂ lattice. The results obtained in the XPS reveals that the Cu ions are successfully substituted in the regular lattice site of SnO₂ without formation of any impurity phases such as Cu or Cu₂O.

Photocatalytic studies

Absorbance and degradation test

MB and RhB dyes were used as model organic dyes in the photocatalytic activity of pure and Cu doped SnO₂ catalyst

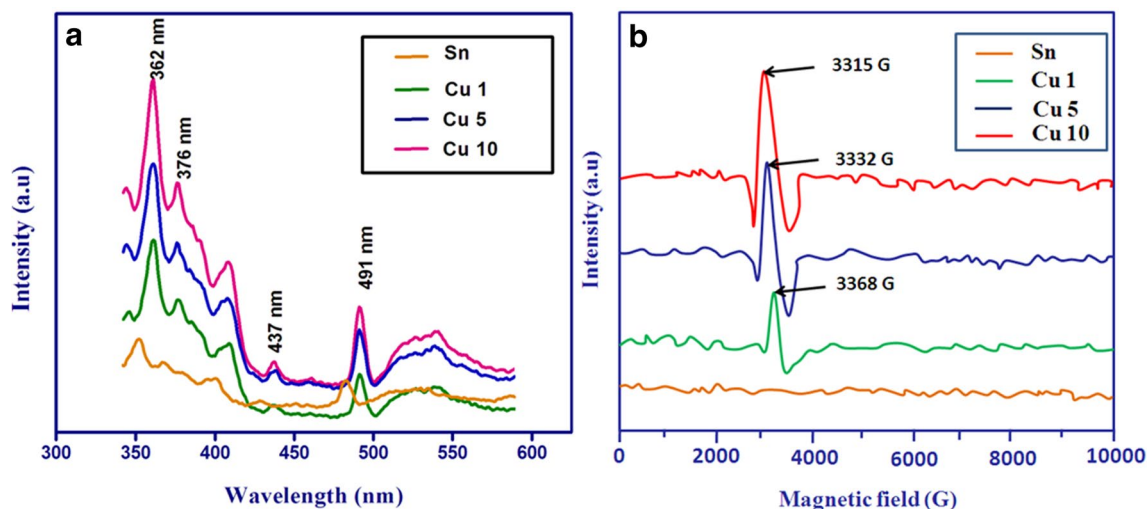


Fig. 5 **a** Photoluminescence spectra of pure and Cu doped SnO₂ nanoparticles; **b** EPR spectra of pure and Cu doped SnO₂ nanoparticles

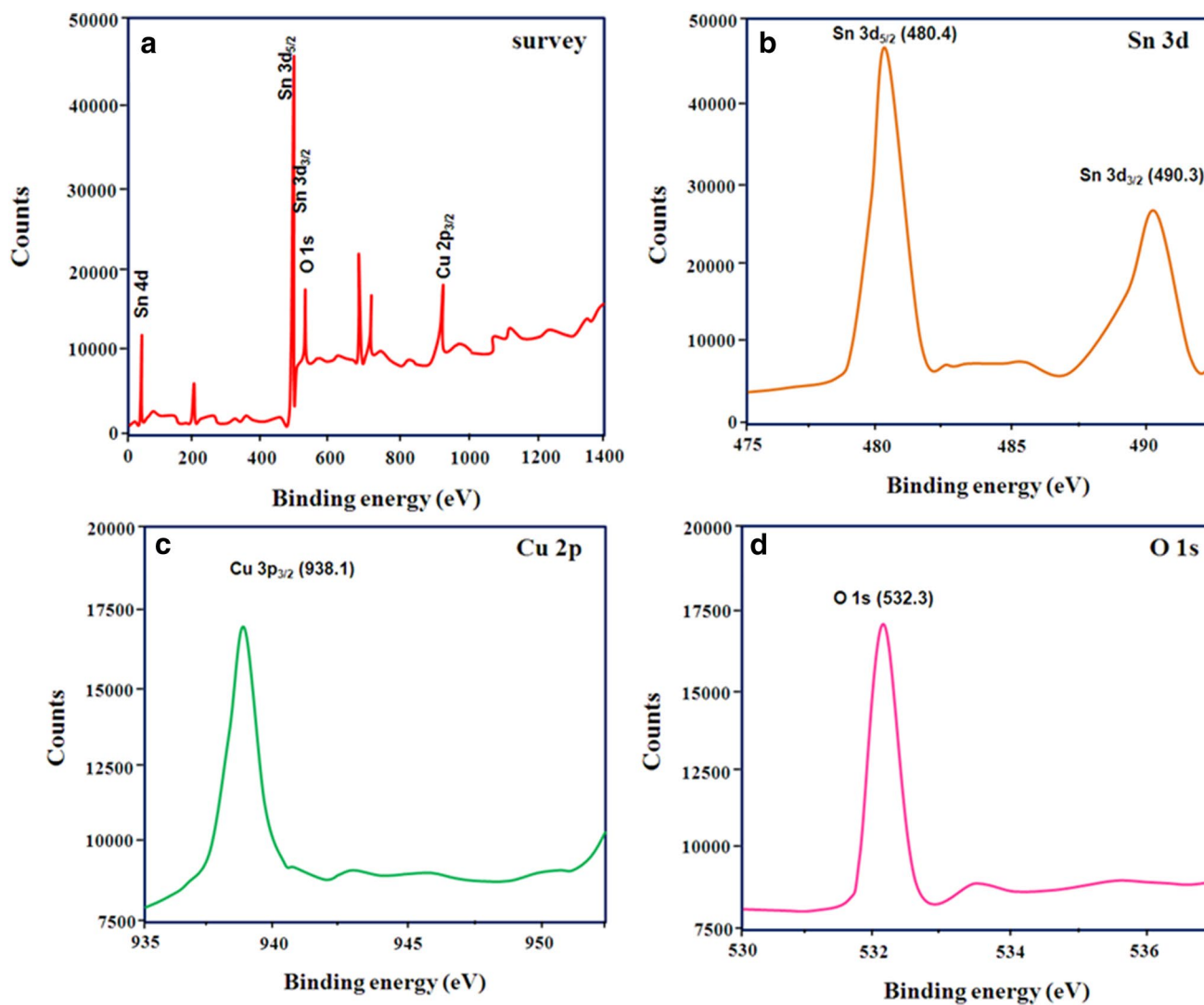


Fig. 6 High-resolution XPS spectra of Cu doped SnO₂ (Cu 10) sample. **a** Survey, **b** Sn 3d, **c** Cu 2p, **d** O 1s

powders under visible light irradiation. For the analyze of visible light absorbance of the characteristic peak of the MB dye at ~ 664 nm and ~ 554 nm for RhB dye was selected as the reference peak. The corresponding UV absorption graphs of the catalyst are illustrated in Fig. 7a–d. It can be seen that the absorption intensity of MB and RhB dyes continuously decreases, and the peak almost disappeared within 120 min. It is noted that the color of the MB was changes initial dark blue, later light blue, and the last stage turns to transparent at 120 min illumination of visible light. Likewise, the color of RhB dye solution was changes from pink color to transparent pink. Therefore, the material is observed to be photocatalytically active. As observed, Cu 10 sample shows the highest photocatalytic activity compared to other samples (Sn, Cu 1 and Cu 5). Numerous experiments were also carried out to explore the photocatalytic activity of the Cu–SnO₂ catalyst. The temporal degradation profile of MB and RhB with the Cu–SnO₂ catalyst sample under visible light irradiation was investigated for various time intervals and the spectra was depict in Fig. 7e, f. It was noticed that Cu 10 samples showed better photocatalytic activities compared to those of Sn, Cu 1 and Cu 5 samples. This could be explained by the following reasons: (1) a appropriate amount of Cu can capably capture the photo-induced electrons. (2) The increase in amount of surface hydroxyl radicals. (3) The absorption edge is considerably shifted to the UV light range. (4) Band gap narrowing. The degradation efficiency of MB was found as 45, 52, 63 and 85% for Sn, Cu 1 Cu 5 and Cu 10 samples, respectively. Similarly the degradation efficiency of RhB was found to be 54, 62, 76 and 92% for Sn, Cu 1 Cu 5 and Cu 10 samples, respectively.

Kinetic studies

Further the kinetics of dye degradation was investigated. The kinetics models of the pseudo-first-order model were experienced to find out the kinetics rate in the degradation of MB and RhB dye solutions by using Cu–SnO₂ catalyst powder. The plot of $\ln(C_t/C_0)$ vs. time is shown in Fig. 7g, h. The linear relationship of the plot of $\ln(C_t/C_0)$ vs. time indicates that the photodegradation of the dye obeys pseudo-first-order kinetics and the rate expression is given by the equation [26]:

$$\ln(C_t/C_0) = kt,$$

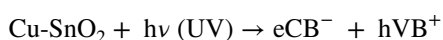
where k is the photodegradation rate constant (min^{-1}) and C_0 and C_t are the concentrations (mg/L) of dye after self-photolysis and at different irradiation times, respectively. The rate constants obtained evidently indicates that the Cu 10 catalyst had faster (see Table 2) that other samples (Sn, Cu1, Cu3 and Cu 5), which could be attributed to the large surface area and smaller band gap of the sample.

Recycle test

We expect, these specific morphology of Cu–SnO₂ nano-structures have long-term stability to exploit their advantages in practical industrial applications. In the practical point of view, stability and recyclability is most important factors in the photocatalysts. Hence, all the catalytic samples were investigated for reusability test for both MB and RhB dye solution with multiple cycles as shown in Fig. 8a, b. In each cycle, the catalyst was centrifuged and washed with distilled water and ethanol until a clear equilibrium solution was obtained. The photocatalyst exhibited a slight loss of efficiency after seven cycles, which could mainly be attributed to the loss of the photocatalyst during the washing in between the cycles. So this would be promising material for high performance photocatalyst and waste water treatment.

Photocatalytic mechanism

The photocatalytic mechanism of pure and Cu doped SnO₂ catalyst with RhB under visible light was shown in Fig. 8c. Generally, photocatalytic degradation process starts with the making of a (e^-/h^+) pair. When the light illuminate on the semiconductor surface, the electrons in the valance band excited to conduction band then the positive holes are leaving in the valance band. These photo-induced pairs are move separately to the surface of the Cu–SnO₂ catalysts, and react with the O₂, OH⁻ concerned in the dye solutions, leading to the formation of superoxide radical anions ($\cdot\text{O}_2^-$) and hydroxyl radicals ($\cdot\text{OH}$) [27]. These radicals are the reactive oxygen species (ROS) in photocatalytic oxidation processes. It can be attack with in the RhB dye solution on the Cu–SnO₂ surface, which results in the degradation of the dye solution. Here, the improved photocatalytic activity of Cu doped SnO₂ may be attributed to the intermediated energy level was formed between the conduction and valance band of pure SnO₂ by Cu doping. Moreover, the high surface area and smaller band gap energy is another crucial role, which can act as a mediator of interfacial charge transfer, thus leading to a high separation rate of photo-induced charge carriers. The band gap energy is lowered in Cu doped samples compared with pristine SnO₂, the energy of UV light can generate more e^+h^- couples resulting in the higher photocatalytic activity.



In the schematic illustration, photo generated electrons are transferred from the valance band to the conduction band of undoped SnO₂ under UV illumination (process I). In Cu–doped SnO₂, substitution of Cu²⁺ ions with Sn⁴⁺ ions in SnO₂ host lattice lowers the conduction band of SnO₂. As a result, in Cu doped SnO₂ samples, electrons can be excited simultaneously from the valance band to Cu energy level. In

Fig. 7 Shows the UV light absorbance of MB ($\lambda_{\text{max}} = 464 \text{ nm}$) as a function of irradiation time. **a** Pure SnO_2 , **b** Cu 10: absorbance spectra of RhB ($\lambda_{\text{max}} = 464 \text{ nm}$) as a function of irradiation time **c** pure SnO_2 , **d** Cu 10; **e** temporal degradation profile of MB **f** degradation profile of RhB for pure and Cu doped SnO_2 , **g** kinetic fit for the degradation of MB, **h** kinetic fit for the degradation of RhB under visible light irradiation

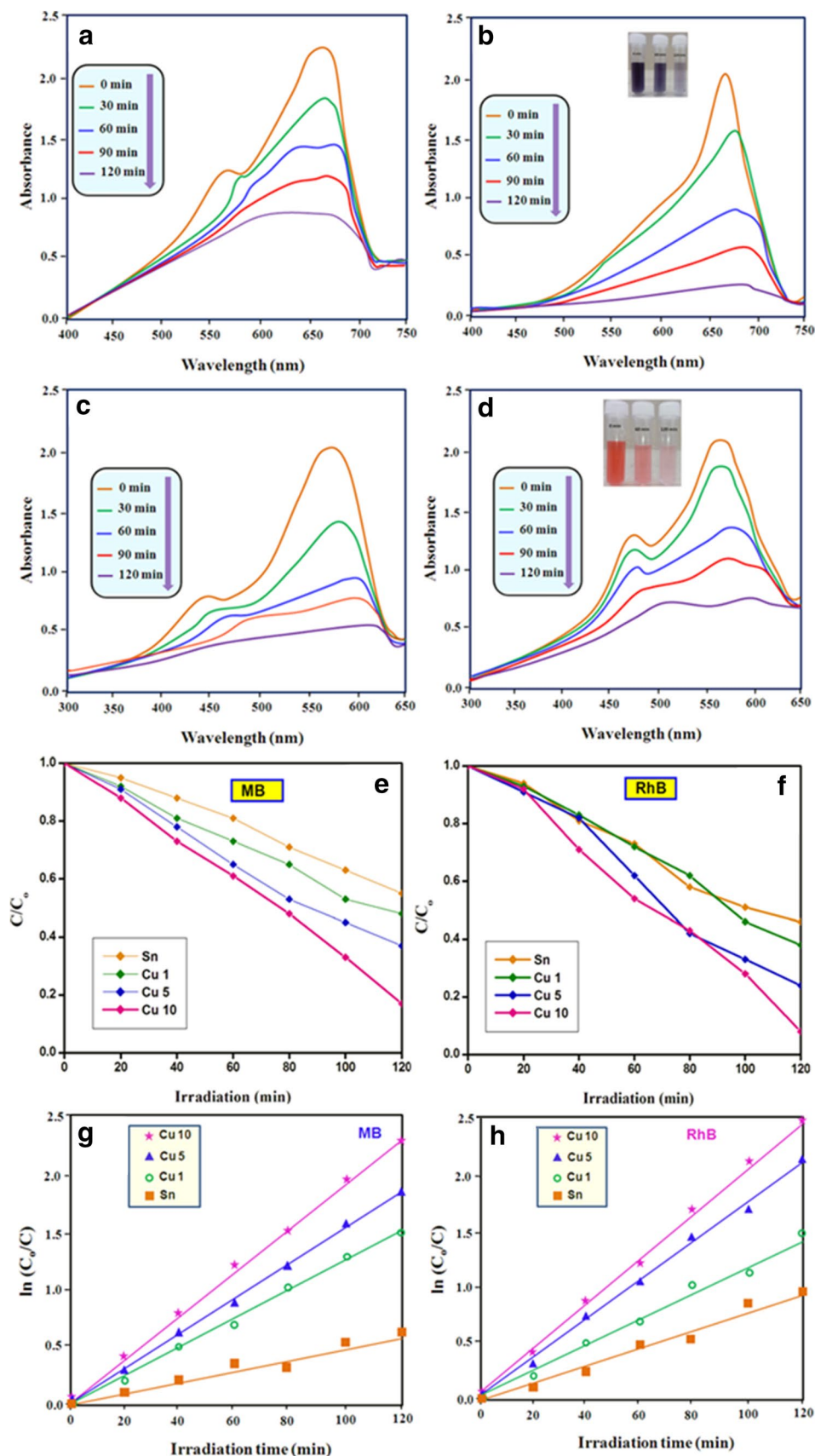


Table 2 Comparison of band gap energy, rate constant and photocatalytic degradation efficiency of pure and Cu doped SnO₂

| Samples | Band gap (eV) | Rate constant of MB | | Rate constant of RhB | | Degradation efficiency at 120 min | |
|---------|---------------|------------------------|-------|------------------------|-------|-----------------------------------|-----|
| | | K (h ⁻¹) | R^2 | K (h ⁻¹) | R^2 | MB | RhB |
| Sn | 3.66 | 0.101 | 0.978 | 0.121 | 0.981 | 45 | 54 |
| Cu 1 | 3.54 | 1.167 | 0.967 | 1.195 | 0.988 | 52 | 62 |
| Cu 5 | 3.42 | 4.434 | 0.991 | 4.489 | 0.993 | 63 | 76 |
| Cu 10 | 3.28 | 6.678 | 0.997 | 7.002 | 0.998 | 85 | 92 |

addition, the photo generated electrons can easily be transferred from the conduction band and the Cu doping energy level to the surface of photocatalyst to capture adsorbed O₂ which improves separation efficiency of charge carriers. Hence, the Cu doped SnO₂ showed superior photocatalytic performance than pure SnO₂. The catalyst was again tested for UV light illumination under the same experimental condition. The source of the UV light is 500 W UV-LED light bulbs. Figure 8d depicts, the change in absorption spectra of RhB using Cu 10 catalyst under UV light illumination. The time interval of irradiation time was 10 min. It was noted that the absorption intensity was drastically decreases with the increase of irradiation time. After 60 min irradiation, the absorption intensity was completely disappear, hence it has photo active under UV light. Further, the degradation efficiency was carried out under same experimental condition. Figure 8e shows the degradation efficiency test of all the catalyst powders. The degradation efficiency was found as 68, 77, 85 and 96% for Sn, Cu1, Cu 5 and Cu 10, respectively. The improved photocatalytic performance of Cu 10 is due to high surface area, which results in enhancing the absorption property of the UV light on its more active surface. To investigate the advantage of the catalyst and its applicability, reuse cycles of photocatalysts were tested for photodegradation of RhB (Fig. 8f). The recycling tests confirmed that a photocatalyst was reasonably stable, there is no decrease in activity in the first three cycles was observed. But, the photocatalytic activity was decreased to 93% after

seven cycles. In general, Cu 10 catalyst is stable and can be recycled with a slight loss of their photochemical activity both UV and visible light irradiation.

Conclusions

In summary, we have reported a simple and one-step microwave irradiation process to synthesis of high quality Cu doped SnO₂ nanorods and studied their structural, optical and photocatalytic properties. XRD result suggest that Cu doped SnO₂ exhibited a tetragonal rutile structure similar to that of undoped SnO₂ with no trace of any other crystallize oxide phase. TEM and SAED pattern confirms the high quality single crystalline with large surface area nanorods of Cu doped SnO₂. Presence of Cu was evidenced by Raman, EDS and ESR analyses the intensity of the corresponding features increasing monotonously with the Cu content. The photocatalytic activity of MB and RhB was significantly improved by Cu doping, this can be ascribed to the reduction of band gap and high surface area, which results in the photogenerated electrons and holes are separated easily and the surface charge carrier transfer rate is improved. Hence this novel method may be gladly extended to the conning of other highly efficient semiconducting oxide photocatalysts for technological applications.

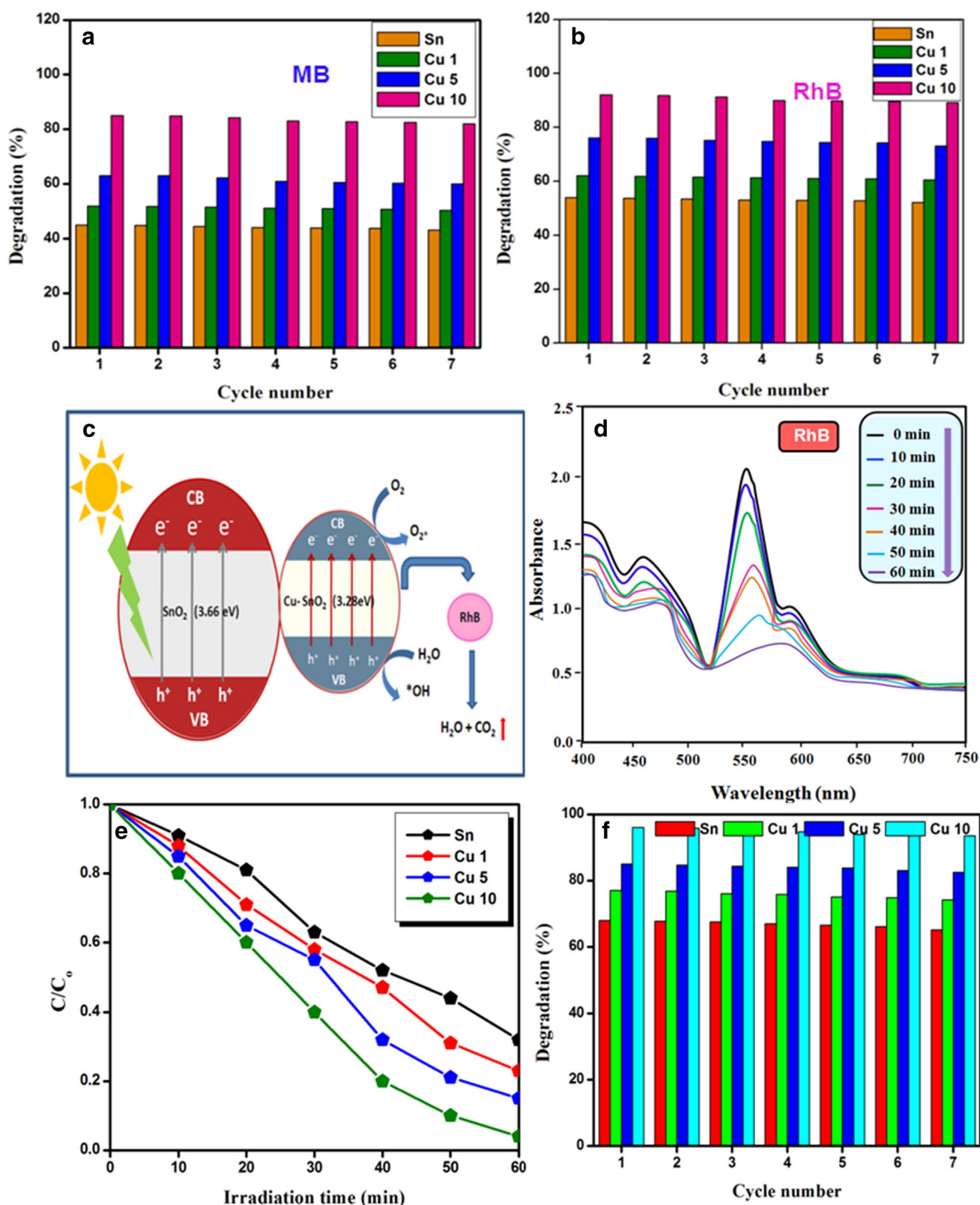


Fig. 8 **a** Recycling test for MB. **b** RhB by using pure and Cu–SnO₂ catalyst. **c** Photocatalytic mechanism of RhB under visible light irradiation. **d** UV absorption spectra of RhB using Cu 10 catalyst under UV light. **e** Degradation test. **f** Recycling test

Compliance with ethical standards

Conflict of interest The authors declare that there is no conflict of interest regarding the research work reported in this manuscript.

References

1. G.C. Collazzo, E.L. Foletto, S.L. Jahn, M.A. Villetti, *J. Environ. Manage.* **98**, 107 (2012)
2. J. Yang, X. Zhang, C. Wang, P. Sun, L. Wang, B. Xia, Y. Liu, *Solid State Sci.* **14**, 139 (2012)
3. C. Karunakaran, V. Rajeswari, P. Gomathisankar, *Solid State Sci.* **13**, 923 (2011)
4. M. Qamar, Z.H. Yamani, M.A. Gondal, K. Alhooshani, *Solid State Sci.* **13**, 1748 (2011)
5. A. Qurashi, Z. Zhong, M.W. Alam, *Solid State Sci.* **12**, 1516 (2010)
6. E.J. Li, K. Xia, S.F. Yin, W.L. Dai, S.L. Luo, C.T. Au, *Mater. Chem. Phys.* **125**, 236 (2011)
7. B. Babu, A.N. Kadam, R.V.S.S.N. Ravikumar, C. Byon, *J. Alloy. Compd.* **703**, 330 (2017)
8. C.V. Reddy, B. Babu, S.P. Vattikuti, R.V.S.S.N. Ravikumar, *J. Shim, J. Lumin.* **179**, 26 (2016)
9. K. Vignesh, R. Hariharan, M. Rajarajan, A. Suganthi, *Solid State Sci.* **21**, 91 (2013)
10. M. Davis, F. Hung-Low, W.M. Hikal, L.J. Hope-Weeks, *J. Mater. Sci.* **48**, 6404 (2013)
11. A. Azita Nouri, Fakhria, *Spectrochim. Acta Part A Mol. Biomol. Spectrosc.* **138**, 563 (2015)
12. M. Parthibavarman, K. Vallalperuman, S. Sathishkumar, M. Durairaj, K. Thavamani, *J. Mater. Sci. Mater. Electron.* **25**, 730 (2014)
13. M. Parthibavarman, S. Sathishkumar, S. Prabhakaran, *J. Mater. Sci. Mater. Elec.* **13**, 2341 (2018)
14. M. Parthibavarman, M. Karthik, P. Sathishkumar, R. Poonguzhali, *J. Iran. Chem. Soc.* **15**, 1419 (2018)
15. M. Parthibavarman, V. Hariharan, C. Sekar, V.N. Singh, *J. Optoelect. Adv. Mater.* **12**, 1894 (2010)
16. M. Karthik, M. Parthibavarman, A. Kumaresan, S. Prabhakaran, V. Hariharan, R. Poonguzhali, S. Sathishkumar, *J. Mater. Sci. Mater. Electron.* **28**, 6635 (2017)
17. S.P. Porto, P.A. Fleury, T.C. Damen, *Phys Rev.* **154**, 522 (1967)
18. F.P. Wang, X.T. Zhou, J.G. Zhou, T.K. Sham, Z.F. Ding, *J. Phys. Chem. C* **111**, 18839 (2007)
19. A. Johari, A. Zohari, M.C. Bhatnagar, M. Sharma, *J. Nanosci. Nanotechnol.* **14**, 5288 (2014)
20. A. Bouaine, N. Brihi, G. Schmerber, C. Ulhaq-Bouillet, S. Colis, A. Dinia, *J. Phys. Chem. C* **111**, 2924 (2007)
21. V. Hariharan, S. Radhakrishnan, M. Parthibavarman, R. Dhilipkumar, C. Sekar, *Talanta.* **85**, 2166 (2011)
22. S. Nilavazhagan, S. Muthukumar, M. Ashokkumar, *J. Mater. Sci. Mater. Electron.* **24**, 2581 (2013)
23. L.M. Fang, X.T. Zu, Z.J. Li, S. Zhu, C.M. Liu, L.M. Wang, F. Gao, *J. Mater. Sci. Mater. Electron.* **19**, 868 (2008)
24. V. Kumar, V. Kumar, S. Som, J.H. Neethling, M. Lee, O.M. Ntwaeaborwa, H.C. Swart, *Nanotech.* **25**, 135701 (2014)
25. A. Jagannatha Reddy, M.K. Kokila, H. Nagabhushana, R.P.S. Chakradhar, C. Shivakumara, J.L. Rao, B.M. Nagabhushana, *J. Alloy. Compd.* **509**, 5349 (2011)
26. A. Bokare, A. Sanap, M. Pai, S. Sabharwal, A.A. Athawale, *Colloids Surf B Biointerface.* **102**, 273 (2013)
27. A. Maleki, M. Safari, B. Shahmoradi, Y. Zandsalimi, H. Daraei, F. Gharibi, *Environ. Sci. Pollut. Res.* **22**, 16875 (2015)